# On the Coverage of Multiple-Input Multiple-Output Visible Light Communications [Invited]

Chen Chen, Wen-De Zhong, and Dehao Wu

***Abstract*—Visible light communication (VLC) using multiple-input multiple-output (MIMO) has great potential for future high-data-rate indoor wireless communications. Owing to the dual function of white light-emitting diodes (LEDs), i.e., illumination and communication functions, both the illumination and communication coverages need to be evaluated when implementing an indoor MIMO-VLC system. In this paper, we present a comprehensive investigation of both the illumination and communication coverages of an indoor MIMO-VLC system. Two techniques are applied in the MIMO-VLC system for communication coverage improvement, including a non-Hermitian symmetry orthogonal frequency division multiplexing (NHS-OFDM) modulation scheme and an imaging angle diversity receiver. A general indoor imaging MIMO-VLC system using NHS-OFDM is described and the analytical bit error rate expression of the system is derived. The impact of LED pairing on the communication coverage of an indoor imaging MIMO-VLC system based on NHS-OFDM is also analyzed.**

***Index Terms*—Coverage; Multiple-input multiple-output (MIMO); Visible light communication (VLC).**

## I. Introduction

Due to their high brightness, low power consumption, long lifetime, cost-effectiveness, and small size, white light-emitting diodes (LEDs) are anticipated to gradually replace incandescent and fluorescent lamps for illumination in most indoor environments [1]. Besides illumination, LEDs can also be used as optical transmitters for simultaneous indoor optical wireless communication [2]. LED-based visible light communication (VLC) is a promising complementary technology to traditional radio-frequency (RF) technologies [3]. By exploiting high-speed, bidirectional, and fully networked VLC systems, light fidelity (Li-Fi) can be successfully deployed in typical indoor environments [4]. Compared to widely used wireless fidelity (Wi-Fi), Li-Fi has many advantages such as license-free spectrum, high data rate, low-cost front ends, and operation free of electromagnetic interference [5].

In order to provide sufficient and uniform illumination in a typical indoor environment, multiple LEDs are commonly mounted in the ceiling [6]. Multiple-input multiple-output (MIMO) is a very natural and effective way to increase the capacity of VLC systems by exploiting the existing LEDs [7]. In recent years, MIMO-VLC has attracted tremendous interest, and many investigations on MIMO-VLC have been reported in the literature. In Ref. [8], a $4 \times 4$ MIMO-VLC system using on–off keying (OOK) with a data rate of 50 Mb/s over a distance of 2 m was demonstrated, where a non-imaging receiver (NImR) consisting of four photodiodes was employed. In Ref. [9], Wang *et al.* reported a $2 \times 2$ MIMO-VLC system using single-carrier frequency-domain equalization (SC-FDE) with a total modulation bandwidth of 125 MHz and 4-ary quadrature amplitude modulation (4QAM) mapping, achieving a raw data rate of 500 Mb/s over a distance of 40 cm where a NImR was also used. As we can see, the spectral efficiencies of these non-imaging MIMO-VLC systems are relatively low due to the use of low-order constellations such as OOK and 4QAM. This is because non-imaging MIMO-VLC systems usually suffer from high channel correlation and hence high interchannel interference (ICI), which is mainly caused by the line-of-sight (LOS) transmission characteristic and the small spatial separation of detectors in typical non-imaging receivers [10–12]. So far, several techniques have been proposed to reduce channel correlation in MIMO-VLC systems, including the introduction of power imbalance between different LEDs or blocking some of the links [11], precoding techniques based on singular value decomposition or independent component analysis [12,13], and the use of non-imaging angle diversity receivers [14,15]. Furthermore, imaging-based receivers (ImRs) have been widely applied in indoor MIMO-VLC systems [16]. Since an ImR can decorrelate the channel matrix coefficients and thus reduce the ICI, a relatively high-order constellation can be adopted in an imaging MIMO-VLC system [17,18].

Although extensive work has already been done on the development of indoor MIMO-VLC systems, most of the work focuses on the improvement of data rate and/or the extension of transmission distance; the communication coverage of an indoor MIMO-VLC system has rarely been studied. Compared with its RF counterpart, which can

Manuscript received January 11, 2017; revised April 15, 2017; accepted June 14, 2017; published August 11, 2017 (Doc. ID 284525).

C. Chen (e-mail: chen0884@e.ntu.edu.sg) and W.-D. Zhong are with the School of Electrical and Electronic Engineering, Nanyang Technological University (NTU), 50 Nanyang Avenue, Singapore 639798, Singapore.

D. Wu is with the Microwave and Communication Systems Research Group, School of Electrical and Electronic Engineering, University of Manchester, Sackville Street, Manchester M13 9PL, UK.

https://doi.org/10.1364/JOCN.9.000D31

 

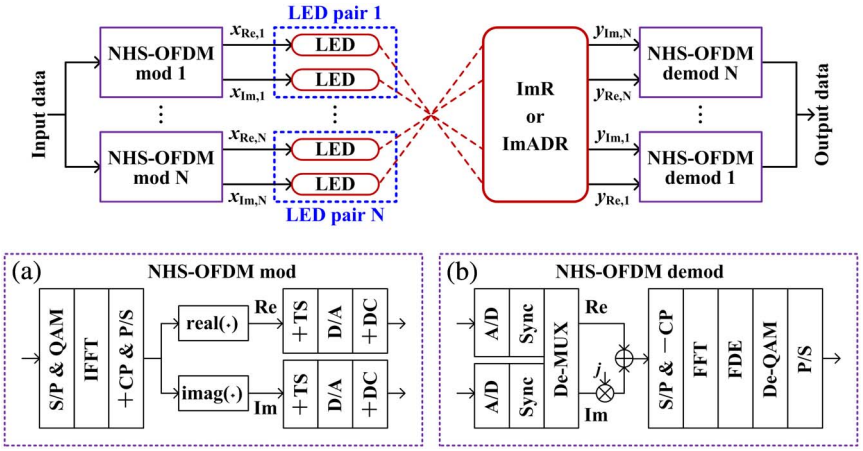


Fig. 1. Schematic diagram of a 2N-channel imaging MIMO-VLC system with N pairs of LEDs using NHS-OFDM. Insets (a) and (b) show the NHS-OFDM modulator (mod) and demodulator (demod), respectively.

easily achieve full coverage of an indoor environment due to the strong multipath effects, it is a challenge for a VLC system to achieve full coverage of an indoor environment due its LOS transmission. In Ref. [19], Vavoulas *et al.* analyzed the communication coverage of an indoor VLC network by considering several factors such as error probability, power consumption, dimming, and node failure. Nevertheless, the coverage issues of indoor MIMO-VLC systems have not been adequately addressed in the literature.

We have recently proposed two techniques to improve the communication coverage area of indoor MIMO-VLC systems, including a non-Hermitian symmetry orthogonal frequency division multiplexing (NHS-OFDM) scheme and a modified ImR. The preliminary results were presented at the IEEE International Conference on Communications (ICC) in 2016 [20]. The superior bit error rate (BER) performance of NHS-OFDM over Hermitian-symmetry-based OFDM (HS-OFDM) in indoor MIMO-VLC systems was further analytically and experimentally verified in Refs. [21,22]. Compared with the non-DC-biased NHS-OFDM schemes as reported in Refs. [23,24], our DC-biased NHS-OFDM scheme is more suitable for practical VLC systems since an appropriate DC bias is added to each LED and therefore a desired illumination level can be guaranteed [25]. Moreover, based on the concept of the modified ImR described in Ref. [20], an imaging angle diversity receiver (ImADR) was proposed for MIMO-VLC systems which can achieve a wider field of view (FOV) and higher optical channel gains (up to 8 dB improvement) than a conventional ImR [26]. In this paper, we extend our previous work [20] and present a comprehensive and in-depth analysis of the illumination and communication coverages of indoor imaging MIMO-VLC systems. The main contributions of this work are summarized as follows:

- We present a general model of indoor imaging MIMO-VLC systems using NHS-OFDM for the first time to our knowledge. In our previous work [20–22], simple two-channel MIMO-VLC systems using NHS-OFDM with one pair of LEDs were evaluated, but a general system model with multiple pairs of LEDs has not yet been studied. In this work, the BER expression of a general indoor imaging MIMO-VLC system using NHS-OFDM is analytically derived.
- We consider both the illumination and communication coverages of indoor imaging MIMO-VLC systems using NHS-OFDM in this work. Analytical and simulation results show that the illumination coverage is mainly affected by two factors, i.e., the LED placement and the LED's maximum luminous intensity. In contrast, the communication coverage is determined by many factors, such as LED placement, LED pairing, LED output optical power, receiver type, etc.
- We analyze the impact of LED pairing on the communication coverage of indoor imaging MIMO-VLC systems based on NHS-OFDM for the first time to our knowledge. Two widely used LED layouts, including square and hexagon, are taken into consideration, and the communication coverage of the system is examined and compared under these two LED layouts.
- Due to its large FOV and high optical channel gain, we apply ImADR in indoor imaging MIMO-VLC systems based on NHS-OFDM. The performance of a conventional ImR and an ImADR is compared and the results show that the system utilizing an ImADR can achieve a larger communication coverage area than that using an ImR. Moreover, the complexity and practical issues of the ImADR are discussed.

As stated before, two different modulation techniques (HS-OFDM and NHS-OFDM) and two different receivers (ImR and ImADR) are compared in MIMO-VLC systems under two different LED placements (square and rhombus). The rest of the paper is organized as follows. Section II introduces the general model of an indoor imaging MIMO-VLC system using NHS-OFDM. In Section III, we derive the analytical BER expression of a general imaging MIMO-VLC system using NHS-OFDM, where both a conventional ImR and an ImADR are applied. The

analytical results in terms of both illumination and communication coverages are presented in Section IV. Finally, Section V concludes the paper.

## II. Imaging MIMO-VLC Using NHS-OFDM

In this section, we present a general model of an indoor imaging MIMO-VLC system using NHS-OFDM. Figure 1 illustrates the schematic diagram of a 2N-channel imaging MIMO-VLC system, where a conventional ImR or an ImADR can be used as the optical receiver. The serial input data of the system are first split into N parallel data streams, and each data stream is then fed into a NHS-OFDM modulator where two outputs are generated. As we can see, 2N LEDs are divided into N pairs and each pair of LEDs is driven by the two outputs of a NHS-OFDM modulator. After free-space propagation, a conventional ImR or an ImADR is employed to detect the optical signal. Both the ImR and the ImADR consist of an imaging lens, an optical filter, and a detector array. The difference between the ImR and the ImADR is discussed in Section II.C. The received N pairs of signals are fed into the respective NHS-OFDM demodulators. The output data can be obtained by combining together the N outputs of the NHS-OFDM demodulators. Although an even number of channels are considered in the imaging MIMO-VLC system due to the pairwise transmission nature of the NHS-OFDM scheme, the obtained results in the following can be easily generalized to an imaging MIMO-VLC system with an arbitrary number of channels. More specifically, when the system has an odd number of channels, a hybrid HS-OFDM/NHS-OFDM approach can be adopted, i.e., the paired LEDs transmit the NHS-OFDM signals while the remaining one LED which is not included in any LED pairs transmits the HS-OFDM signal. Similarly, when one LED in an LED pair is blocked, the other LED in the LED pair can be used to transmit the HS-OFDM signal by adopting the hybrid HS-OFDM/NHS-OFDM approach.

### A. Channel Model

Due to LOS transmission and reflections from surfaces within the room, a receiver can usually detect both LOS and diffuse components of light emitted by the LEDs. It has been verified in Ref. [7] that the weakest LOS component is at least 7 dB higher in electrical power than the strongest diffuse component in typical indoor environments. The diffuse components may be different under different indoor system configurations. In this work, for simplicity of analysis, we only consider the LOS link in the indoor MIMO-VLC system [7]. Throughout this paper, each LED in the MIMO-VLC system means an LED lamp consisting of multiple chips. By modeling the irradiance of an LED chip as a generalized Lambertian radiation pattern [2], the LOS optical channel gain between the $t$-th LED and the $r$-th detector in the detector array of the receiver is calculated by

$$h_{rt} = \sum_{i=1}^{L} \frac{(m+1)A}{2\pi d_{rt_i}^2} \mu\eta \cos^m(\varphi_{rt_i}) \cos(\theta_{rt_i}), \quad (1)$$

where $m = -\ln 2/\ln(\cos \Psi)$ is the Lambertian emission order; $\Psi$ is the LED's semi-angle at half-power; $L$ is the number of LED chips in one LED; $A$ is the detector's active area; $d_{rt_i}$ is the distance between the $i$-th chip in the $t$-th LED and the $r$-th detector; $\mu$ and $\eta$ are the gains of the optical filter and lens, respectively; $\varphi_{rt_i}$ is the emission angle; and $\theta_{rt_i}$ is the incident angle. The gain of the optical lens is given by $\eta = n^2/\sin^2 \Phi$, where $n$ and $\Phi$ are the refractive index and half-angle FOV of the lens, respectively [10]. If the incident light is outside the FOV of the receiver, the LOS optical channel gain $h_{rt}$ becomes zero. It should also be noted that multipath fading in indoor VLC systems can generally be neglected since the typical active area of a detector is much larger than the wavelength of the visible light [2,5].

### B. NHS-OFDM With LED Pairing

Inset (a) of Fig. 1 illustrates the schematic of the NHS-OFDM modulator [20], where the input data stream is serial-to-parallel (S/P) converted and the resultant parallel data are mapped to QAM symbols. After performing the inverse fast Fourier transform (FFT), cyclic prefix (CP) insertion, and parallel-to-serial (P/S) conversion, a serial complex-valued signal is obtained. Considering that only real-valued signals can be transmitted by LEDs [27], the real (Re) and imaginary (Im) parts of the complex-valued signal are separated and two training sequences (TSs) are, respectively, added to the Re and Im parts. After digital-to-analog conversion, two DC bias currents are added and hence two unipolar real-valued signals are generated, which are subsequently used to separately modulate the intensities of a pair of LEDs. In the NHS-OFDM demodulator [20], as shown in inset (b) of Fig. 1, the received Re and Im signals are analog-to-digital converted, which are then separately synchronized, using the corresponding TSs to eliminate the phase imbalance between the Re and Im signals. By exploiting the pre-estimated channel information, MIMO de-multiplexing (De-MUX) is performed to balance the electrical powers of the received Re and Im signals. After that, the resultant Re and Im signals are combined together to reconstruct the complex-valued signal. Subsequently, the transmitted data stream can be recovered via S/P conversion, CP removal, FFT, FDE, QAM de-mapping, and P/S conversion.

It can be clearly observed from Fig. 1 that the signals are transmitted in pairs in indoor MIMO-VLC systems based on NHS-OFDM. Hence, it is necessary to divide the individual LEDs into pairs when there are multiple LEDs in the ceiling. The way that the LEDs are paired is associated with the layout of the LEDs in the ceiling. Several LED layouts have been studied, where square and hexagon are the most-used LED layouts in indoor VLC systems [6,28]. Thus, square and hexagonal LED layouts are considered here. Figures 2(a) and 2(b) depict the cluster formation in square and hexagonal LED layouts, respectively. It can

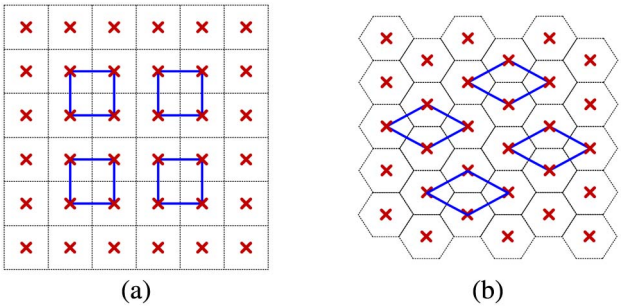


Fig. 2. Cluster formation in (a) square and (b) hexagonal LED layout where a red "×" indicates an LED.

be seen from Fig. 2(a) that the square layout can be divided into multiple square clusters, and each cluster consists of four LEDs placed in a square. Similarly, as shown in Fig. 2(b), the hexagonal layout can be divided into multiple rhombic clusters, each also consisting of four LEDs placed in a rhombus. Therefore, both the square and rhombic clusters consist of two pairs of LEDs.

Figure 3 illustrates the LED pairing schemes in square and rhombic clusters. Considering geometric symmetry, the four LEDs in a square cluster can be paired in two ways: one is parallel pairing and the other is cross pairing. For parallel pairing, as shown in Fig. 3(a), two adjacent LEDs are paired together and two pairs of LEDs are parallel with each other in the square cluster. However, for cross pairing, two LEDs in the opposite corners are paired together and two pairs of LEDs cross with each other, as shown in Fig. 3(b). Similarly, it can be seen from Figs. 3(c) and 3(d) that four LEDs in a rhombic cluster can also be parallel or crosswise paired.

### C. ImR Versus ImADR

As an effective way to reduce channel correlation and thus improve system capacity, imaging-type receivers have

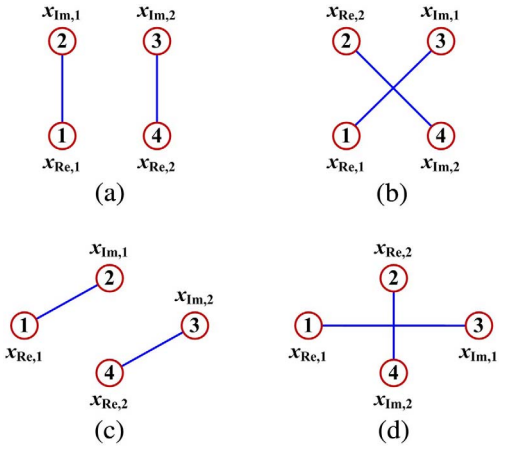


Fig. 3. LED pairing: (a) parallel pairing in a square cluster, (b) cross pairing in a square cluster, (c) parallel pairing in a rhombic cluster, and (d) cross pairing in a rhombic cluster.

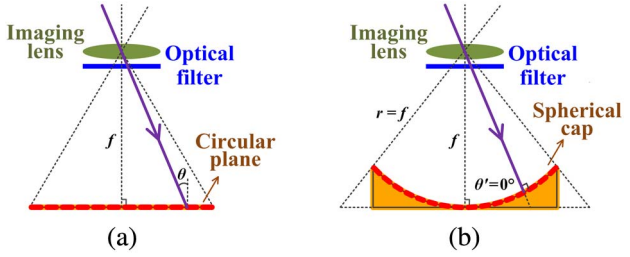


Fig. 4. Side views of (a) conventional ImR with vertically oriented detectors and (b) ImADR with angle diversity detectors.

been widely explored in indoor MIMO-VLC systems. Figures 4(a) and 4(b) show the side views of a conventional ImR and an ImADR, respectively. Both the conventional ImR and the ImADR consist of an imaging lens, an optical filter, and a detector array. The imaging lens is employed to project the incident light from the LEDs onto the detector array, while the optical filter is used to attenuate the unwanted ambient light. The FOV of the ImR or the ImADR should be large enough such that the light emitted by all LEDs in the MIMO-VLC system can be detected by the receiver. Note that in this paper, the analysis and simulation are based on paraxial optics approximation. As shown in Fig. 4(a), the ImR has a two-dimensional circular detector array which consists of vertically oriented detectors. The FOV of the ImR is limited by the size of the circular detector array [17]. Moreover, the incident angle $\theta$ of an incident light is determined by the relative positions of the corresponding LED and detector. It can be observed that the incident angle is relatively large when the corresponding detector is near the edge of the detector array, indicating a small optical channel gain. Unlike the ImR, a three-dimensional spherical-cap-shaped detector array consisting of angle diversity detectors is adopted in the ImADR [26]. For fair comparison, the ImR and ImADR are assumed to use the same detectors in the detector array. That is, each detector in the ImADR has the same physical area as that in the ImR. It can be seen from Fig. 4(b) that the radius of the base of the three-dimensional spherical-cap-shaped detector array is equal to the focal length of the lens, i.e., $r = f$. Hence, when an ImR and an ImADR have the same horizontal size, the ImADR has a much larger FOV than the ImR. Moreover, since the imaging lens is placed at the center of the spherical-cap-shaped detector array and $r = f$, the incident angle $\theta'$ is always 0°, which is independent from the positions of the corresponding LED and detector. Therefore, the LOS optical channel gain using an ImADR is obtained by

$$h_{rt}^{*} = \sum_{i=1}^{L} \frac{(m+1)A}{2\pi d_{rt_i}^2} \mu\eta \cos^m(\varphi_{rt_i}). \tag{2}$$

As per Eqs. (1) and (2), the ImADR can achieve higher optical channel gains than the conventional ImR. More details about ImADR can be found in Ref. [26].

In an imaging MIMO-VLC system with a number of LEDs in the ceiling, the same number of light spots can be observed on the detector array of the receiver and each

light spot may cover multiple adjacent detectors. To obtain a final output signal from the multiple output signals, the optical channel gains between the LED and the detectors in the detector array are first calculated. Then, an adequate threshold level can be set to exclude those detectors that are not covered by the light spot. After that, the resultant signals coming from the detectors that are covered by the light spot can be further processed to get a final output via diversity combining [29].

Compared with the conventional ImR which has a two-dimensional planar detector array, the ImADR employing a three-dimensional spherical-cap-shaped detector array has relatively high complexity and cost. Nevertheless, with the rapid development of CMOS technology, we believe that the complexity and cost for manufacturing ImADRs will become acceptable and the advantages, including improved FOV and optical channel gain, will make ImADR a promising candidate for high-speed VLC systems.

### D. Coverage

Considering the dual function of LEDs, i.e., illumination and communication, the coverage of an indoor MIMO-VLC system can be defined in two ways. One is the illumination coverage, defined by the covered area within which the horizontal illuminance is no less than a threshold. Assuming that there are a total of $N_t$ LEDs mounted in the ceiling of a room, the horizontal illuminance at the location of a user in the receiving plane is calculated by [30]

$$E_h = \sum_{i=1}^{N_t} \frac{I_0 \cos^m(\varphi_i)\cos(\theta_i)}{d_i^2}, \tag{3}$$

where $I_0$ is the maximum luminous intensity of the LED; $m$ is the Lambertian emission order which is the same as in Eq. (1); $\varphi_i$ and $\theta_i$ are the corresponding emission and incident angles, respectively; and $d_i$ is the distance between the $i$-th LED and the user's location. According to the European lighting standard, the minimum required illuminance for reading in indoor environments is 400 lx [31]. Hence, the threshold for obtaining the illumination coverage can be set to 400 lx. The other way to define the coverage of an indoor MIMO-VLC system is the communication coverage [20]. For a 7% forward error correction overhead, corresponding to a BER threshold of $3.8 \times 10^{-3}$, the communication coverage can be defined by the covered area within which the BER is less than $3.8 \times 10^{-3}$.

## III. BER Analysis

We analytically derive the BER expression of a general imaging MIMO-VLC system using the NHS-OFDM scheme. For simplicity and without loss of generality, we consider a 2N-channel imaging MIMO-VLC system in a typical indoor environment. Both a conventional ImR and ImADR are analyzed in the 2N-channel imaging MIMO-VLC system. It is assumed that the 2N LEDs have the same output optical power $P_{\text{opt}}$ and the same modulation index $\xi$, and meanwhile all the detectors in the detector array of the receiver (ImR or ImADR) have the same responsivity $R$. By dividing the total 2N individual LEDs into N pairs, as discussed in Section II.B, the transmitted optical signal vector of the $i$-th pair of LEDs (LED $2i-1$ and LED $2i$) is represented by

$$\mathbf{s}_i = P_{\text{opt}}(1 + \xi \mathbf{x}_i), \tag{4}$$

where $\mathbf{x}_i = [x_{\text{Re},i} \quad x_{\text{Im},i}]^T$ is the modulating signal vector. $x_{\text{Re},i}(t)$ and $x_{\text{Im},i}(t)$ are, respectively, the normalized Re and Im parts of the complex-valued signal, i.e., $x_i(t) = x_{\text{Re},i}(t) + j \times x_{\text{Im},i}(t)$, which is generated from the $i$-th NHS-OFDM modulator. We assume that LED $2i-1$ and LED $2i$ transmit the Re and Im parts of the complex-valued signal, respectively. After indoor free-space propagation, the light is detected by an ImR or ImADR and the received electrical signal vector is given by

$$\mathbf{y}_i = RP_{\text{opt}}\xi \mathbf{H}\mathbf{x}_i + \mathbf{n}_i, \tag{5}$$

where $\mathbf{H}$ is the channel matrix and $\mathbf{n}_i$ is the additive noise vector. $\mathbf{H}$ has a dimension of $(k_1 + k_2) \times 2$, where $k_1$ and $k_2$ are the numbers of detectors that are covered by the two light spots corresponding to LED $2i-1$ and LED $2i$, respectively. Although an imaging MIMO system might not be completely ICI-free since the projected light spots on the detector array might overlap with each other [32], the detectors which are located in the overlapping area can be excluded due to their substantially reduced signal-to-noise ratios (SNRs). Hence, for simplicity of analysis and without loss of generality, we assume that the imaging MIMO-VLC system using an ImR or an ImADR in the following analysis is ICI-free and the channel matrix can be represented by a diagonal matrix [17]. When an ImR is used, the optical channel gain can be calculated as per Eq. (1), and hence the diagonal channel matrix $\mathbf{H}$ is expressed by

$$\mathbf{H}_{\text{ImR}} = \text{diag}(\underbrace{h_{1,2i-1}, \ldots, h_{k_1,2i-1}}_{\text{Re part}}, \underbrace{h_{k_1+1,2i}, \ldots, h_{k_1+k_2,2i}}_{\text{Im part}}). \tag{6}$$

However, when an ImADR is used, the optical channel gain is given by Eq. (2). Therefore, $\mathbf{H}$ becomes

$$\mathbf{H}_{\text{ImADR}} = \text{diag}(\underbrace{h^*_{1,2i-1}, \ldots, h^*_{k_1,2i-1}}_{\text{Re part}}, \underbrace{h^*_{k_1+1,2i}, \ldots, h^*_{k_1+k_2,2i}}_{\text{Im part}}). \tag{7}$$

Substituting Eqs. (6) and (7) into Eq. (5) yields the received electrical signal vectors of the 2N-channel imaging MIMO-VLC system using ImR and ImADR, respectively. Moreover, the noise vector $\mathbf{n}_i$ is given by $\mathbf{n}_i = [n_{\text{Re},i} \quad n_{\text{Im},i}]^T$, where $n_{\text{Re},i}(t)$ and $n_{\text{Im},i}(t)$ can both be modeled as real-valued additive white Gaussian noises (AWGNs), each consisting of shot noise and thermal noise. The detailed expressions of the variances of the shot and thermal noises can be found in [2].

In order to recover the transmitted data from the received signals, MIMO De-MUX is performed and the demultiplexed signals are further normalized. Zero-forcing

using basic channel inversion is adopted for MIMO De-MUX due to its low complexity [8]. Hence, the estimate of the transmitted signal vector is given by

$$\tilde{\mathbf{x}}_i = \frac{1}{RP_{\text{opt}}\xi}\mathbf{H}^{-1}\mathbf{y}_i = \mathbf{x}_i + \frac{1}{RP_{\text{opt}}\xi}\mathbf{H}^{-1}\mathbf{n}_i. \tag{8}$$

As we know, each light spot may cover multiple detectors in the detector array and multiple output signals carrying the same data can be obtained. Thus, diversity combining can be performed to generate a final output signal. In this analysis, select-best combining (SBC) is adopted for the sake of simplicity [30]. Note that better SNR performance might be achieved by exploiting more detectors with effective signal processing. When using SBC, the detector with the highest SNR is selected. After diversity combining, the Re and Im signals from two light spots can be obtained by

$$\begin{cases} \tilde{x}_{\text{Re},i} = \arg\max\limits_{\tilde{x}_{ij}}\{\text{SNR}(\tilde{x}_{ij})\}, & 1 \le j \le k_1 \\ \tilde{x}_{\text{Im},i} = \arg\max\limits_{\tilde{x}_{ij}}\{\text{SNR}(\tilde{x}_{ij})\}, & k_1+1 \le j \le k_1+k_2 \end{cases}, \tag{9}$$

where $\text{SNR}(\tilde{x}_{ij})$ is the estimated SNR of $\tilde{x}_{ij}(t)$, which is the $j$-th element of $\tilde{\mathbf{x}}_i$. As per Eq. (9), the corresponding optical channel gains can also be attained by

$$\begin{cases} h_{\text{Re},i} = \arg\max\limits_{h_{ij}}\{\text{SNR}(\tilde{x}_{ij})\}, & 1 \le j \le k_1 \\ h_{\text{Im},i} = \arg\max\limits_{h_{ij}}\{\text{SNR}(\tilde{x}_{ij})\}, & k_1+1 \le j \le k_1+k_2 \end{cases}, \tag{10}$$

where $h_{ij}$ is the $j$-th diagonal element of $\mathbf{H}$.

Therefore, the complex-valued signal at the input of the $i$-th NHS-OFDM demodulator can be reconstructed by

$$\tilde{x}_i = \tilde{x}_{\text{Re},i} + j \times \tilde{x}_{\text{Im},i}. \tag{11}$$

According to Eq. (11), the SNR of the received complex-valued signal is calculated by [22]

$$\text{SNR}_i = \frac{2(RP_{\text{opt}}\xi h_{\text{Re},i}h_{\text{Im},i})^2}{h_{\text{Im},i}^2\sigma_{\text{Re},i}^2 + h_{\text{Re},i}^2\sigma_{\text{Im},i}^2}, \tag{12}$$

where $\sigma_{\text{Re},i}^2$ and $\sigma_{\text{Im},i}^2$ are the variances of $n_{\text{Re},i}(t)$ and $n_{\text{Im},i}(t)$, respectively. The analytical BER expression of an OFDM system using $I \times J$ rectangular QAM mapping over an AWGN channel can be approximated by [33]

$$\text{BER} = \frac{2}{\log_2(I \times J)}\left(\frac{I-1}{I} + \frac{J-1}{J}\right)Q\left(\sqrt{\frac{6 \times \text{SNR}}{I^2+J^2-2}}\right), \tag{13}$$

where $Q(\cdot)$ denotes the $Q$ function. Substituting Eq. (12) into Eq. (13) yields the BER, i.e., $\text{BER}_i$, obtained at the output of the $i$-th NHS-OFDM demodulator. Finally, the average BER of the 2N-channel imaging MIMO-VLC system using NHS-OFDM is given by

$$\text{BER}_{\text{av}} = \frac{1}{\text{N}}\sum_{i=1}^{\text{N}}\text{BER}_i. \tag{14}$$

It should be noted that the BER performance of an indoor imaging MIMO-VLC system using NHS-OFDM is affected by the way the LEDs are paired, as discussed in Section II.B. The preceding analysis is applicable to the system exploring different LED pairing schemes. Moreover, although we only consider NHS-OFDM in the analysis, the BER performance of an imaging MIMO-VLC system using HS-OFDM can be achieved in a similar way, as derived in [22].

## IV. Results and Discussion

In this section, we evaluate the performance of an indoor imaging MIMO-VLC system using NHS-OFDM with an ImR or an ImADR, in terms of illumination and communication coverages. As discussed in Section II.B, the ceiling LEDs in a general MIMO-VLC system, with either a square or hexagonal layout, can be divided into multiple LED clusters each consisting of four LEDs. Thus, a four-channel imaging MIMO-VLC system is analyzed in the following and two LED placements are considered, including a square and a rhombic placement. The key parameters of the MIMO-VLC system are listed in Table I. A typical room with dimensions (length × width × height) of 5 m × 5 m × 3 m is considered, and the height of the receiving plane is 0.85 m. All four LEDs have the same semi-angle at half power of 60° and each LED consists of four chips. The modulation index is 0.3 and the modulation bandwidth is set to 20 MHz. Although the 3 dB bandwidth of a phosphor-coated white LED is only several MHz, the modulation bandwidth can be increased using pre-FDE techniques [34,35]. 16QAM ($I = 4, J = 4$) mapping is adopted in NHS-OFDM modulation and demodulation. Thus, the raw data rate achieved in this four-channel MIMO-VLC system is $4 \times \log_2 16 \times 20 = 320$ Mb/s. The gain of the optical filter is 0.9. The diameter and the focal length of the optical lens are 10 and 12 mm, respectively. The optical lens has a refractive index of 1.5 and a half-angle FOV of 72°. It is assumed that the detector array in the ImADR is large enough to achieve full coverage of the room. Each detector has a diameter of 1 mm and a responsivity of 0.53 A/W, and the detector separation is set to 2 mm. The background current is 58 μA. For the purpose of

TABLE I
Key Parameters of the MIMO-VLC System

| Parameter | Value |
|---|---|
| Room dimensions (length × width × height) | 5 m × 5 m × 3 m |
| Height of receiving plane | 0.85 m |
| Semi-angle at half power of LED | 60° |
| Number of chips in LED | 4 |
| Modulation index | 0.3 |
| Modulation bandwidth | 20 MHz |
| QAM order | 16 (4 × 4) |
| Gain of optical filter | 0.9 |
| Diameter of optical lens | 10 mm |
| Focal length of optical lens | 12 mm |
| Refractive index of optical lens | 1.5 |
| Half-angle FOV of optical lens | 72° |
| Diameter of detector | 1 mm |
| Responsivity of detector | 0.53 A/W |
| Background current | 58 μA |

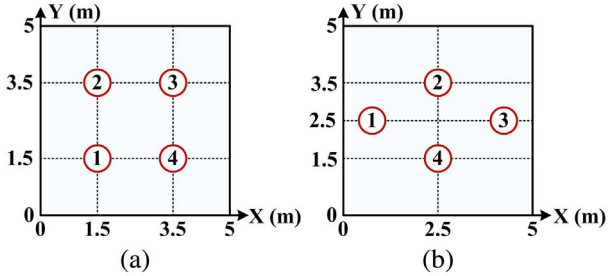


Fig. 5. Two LED placements in the ceiling of a 5 m × 5 m × 3 m room: (a) square and (b) rhombus.

comparison, the performance of a four-channel imaging MIMO-VLC system using HS-OFDM with exactly the same parameters is also investigated.

Figures 5(a) and 5(b) depict the square and rhombic LED placements in the ceiling, respectively. The coordinates of the lower left corner of the floor are set to (0, 0, 0) and the units of all the coordinates are meters. In the square placement, the coordinates of the four LEDs are (1.5, 1.5, 3), (1.5, 3.5, 3), (3.5, 3.5, 3), and (3.5, 1.5, 3), as shown in Fig. 5(a). However, the coordinates in the rhombic placement are given by $(2.5 - \sqrt{3}, 2.5, 3)$, (2.5, 3.5, 3), $(2.5 + \sqrt{3}, 2.5, 3)$, and (2.5, 1.5, 3), as can be seen from Fig. 5(b).

We first evaluate the illumination coverage of the indoor four-channel imaging MIMO-VLC system. Figure 6 shows the illumination coverage at a target illuminance of 400 lx. As we can see, the coverage contours over the receiving plane are different when different LED placements are considered. For a square LED placement, the illumination coverage is covered by the red dot-dash line with an LED maximum luminous intensity of 1500 cd. The illumination coverage is enlarged as covered by the red solid line, when the LED maximum luminous intensity is increased to 2000 cd. For a rhombic LED placement, the illumination coverages are shown by the blue dotted and blue dashed line when the maximum luminous intensities of each LED are 1500 and 2000 cd, respectively. As we can see, the minimum required illuminance for reading can be

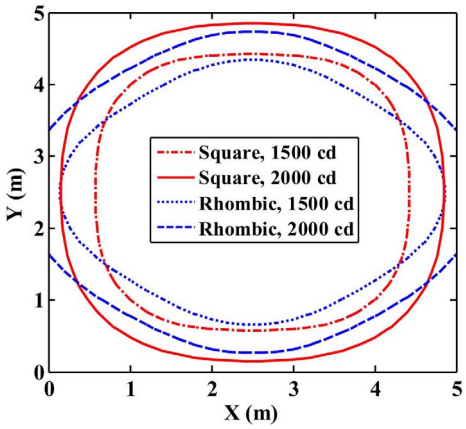


Fig. 6. Illumination coverage of the four-channel imaging MIMO-VLC system at a target illuminance of 400 lx.

achieved in most of the room area when the LED maximum luminous intensity is 2000 cd, although the coverage contours have different shapes under different LED placements. It can be concluded that the illumination coverage of the four-channel imaging MIMO-VLC system is affected by both the LED placement and the LED's maximum luminous intensity.

Next, we analyze the BER performance of the indoor four-channel imaging MIMO-VLC system where two modulation techniques (HS-OFDM and NHS-OFDM), two receivers (ImR and ImADR), and two LED placements (square and rhombus) are considered for performance comparison. In order to verify the BER expression derived in Section III, Monte Carlo simulations are conducted and 2000 HS-OFDM/NHS-OFDM symbols are transmitted for BER measurement. The output optical power of each LED is set to 10 W. Figure 7 shows the BER performance of the four-channel imaging MIMO-VLC system, where the simulation and analytical results are given by markers and lines, respectively. It can be clearly observed that the analytical results agree very well with the simulation results. Figure 7(a) plots the BER versus receiver position offset along the $x$ direction with $y = 2.5$ m for a square LED placement. It can be seen that the same BER performance is obtained for HS-OFDM and parallel-pairing-based NHS-OFDM, while the best BER performance is achieved by NHS-OFDM with cross pairing, using either an ImR or an ImADR. As a general conclusion obtained in [21], NHS-OFDM can outperform HS-OFDM only when two HS-OFDM signals have different SNRs. For $y = 2.5$ m, the HS-OFDM signals from LED 1 and LED 2 (LED 3 and LED 4) have the same SNRs, and hence HS-OFDM and NHS-OFDM have the same BER performance when LED 1 and LED 2 (LED 3 and LED 4) are paired together. However, when cross pairing is adopted, the HS-OFDM signals from LED 1 and LED 2 (LED 3 and LED 4) always have different SNRs along the $x$ direction for $y = 2.5$ m, except $x = 2.5$ m. As a result, NHS-OFDM with cross pairing can achieve much better BER performance than HS-OFDM and NHS-OFDM with parallel pairing. Moreover, due to its high optical channel gain, the system using ImADR attains a substantial BER reduction compared with the system using ImR. However, for $x = 2.5$ m as shown in Fig. 7(b), NHS-OFDM outperforms HS-OFDM along the $y$ direction with either parallel or cross pairing. It is also revealed that NHS-OFDM can achieve the same BER performance with parallel pairing or cross pairing due to the geometric symmetry. In contrast, when the four LEDs are placed in a rhombus, the geometric symmetry no longer exists. As can be seen from Figs. 7(c) and 7(d), NHS-OFDM with cross pairing outperforms NHS-OFDM with parallel pairing, while HS-OFDM has the worst BER performance. As illustrated in Figs. 7(a)–7(d), the BER performance of an MIMO-VLC system using NHS-OFDM largely depends on both the way the LEDs are paired and the type of receivers employed. Considering the impact of both LED pairing and receiver type, we can generally conclude that NHS-OFDM with cross pairing using an ImADR is the best option for the MIMO-VLC system, with either a square or a rhombic LED placement.

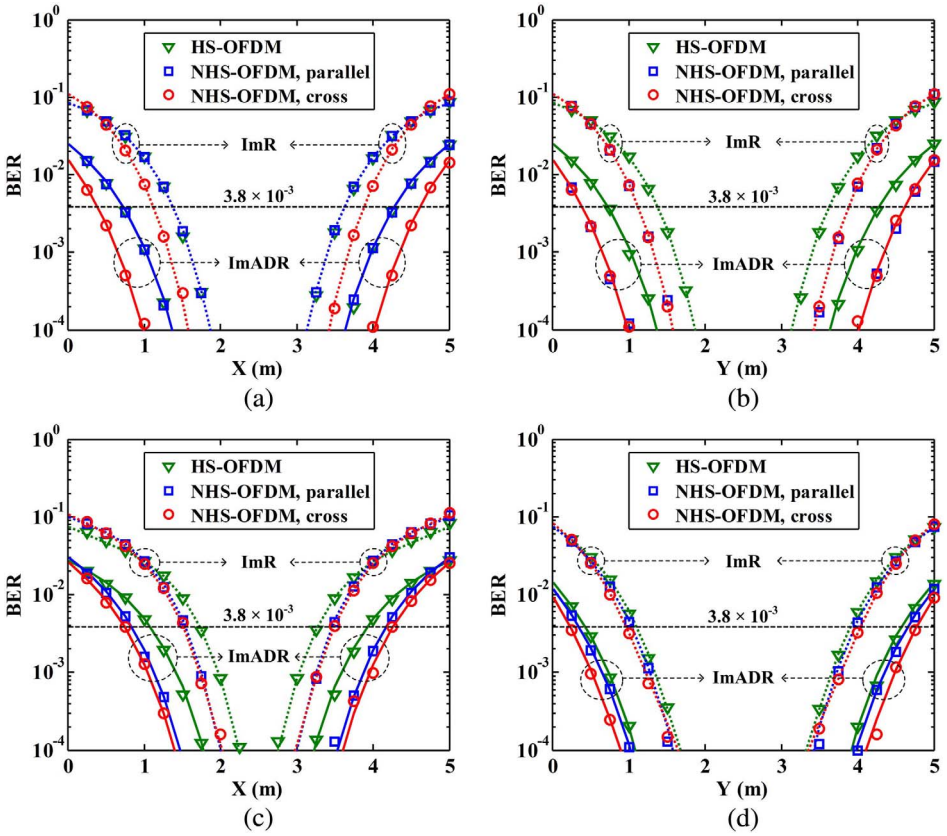


Fig. 7. (a) BER versus $x$ with $y = 2.5$ m for a square LED placement, (b) BER versus $y$ with $x = 2.5$ m for a square LED placement, (c) BER versus $x$ with $y = 2.5$ m for a rhombic LED placement, and (d) BER versus $y$ with $x = 2.5$ m for a rhombic LED placement. The output optical power of each LED is 10 W. Markers show the simulation results and lines give the corresponding analytical results.

The communication coverage of the indoor four-channel imaging MIMO-VLC system at a target BER of $3.8 \times 10^{-3}$ is shown in Fig. 8, where the output optical power of each LED is 10 W. For a square LED placement, the coverage areas using HS-OFDM are shown by the green dotted lines, as shown in Fig. 8(a), while the coverage areas using NHS-OFDM with parallel and cross pairing are shown by the blue dashed and the red solid lines, respectively. As can be seen, the coverage contours using both HS-OFDM and NHS-OFDM with cross pairing can be approximated as circles, while the coverage contours using NHS-OFDM with parallel pairing can be approximated as ellipses.

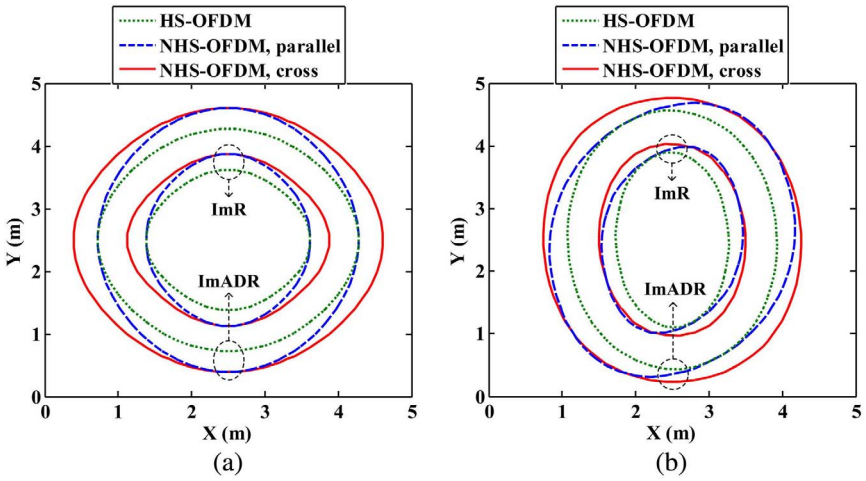


Fig. 8. Communication coverage of the four-channel imaging MIMO-VLC system at a target BER of $3.8 \times 10^{-3}$ for (a) square LED placement and (b) rhombic LED placement. The output optical power of each LED is 10 W.

The area of a circle is calculated by $A_c = \pi r_c^2$, where $r_c$ is the radius of the circle, and the area of an ellipse is given by $A_e = \pi ab/4$, where $a$ and $b$ are the major and minor axes of the ellipse, respectively. When an ImR is used, the coverage circle using HS-OFDM has a radius of 1.1 m, and hence the area is 3.8 $m^2$. By replacing HS-OFDM with NHS-OFDM, the covered area is improved. Specifically, the coverage contour becomes an ellipse when using NHS-OFDM with parallel pairing, indicating that the coverage is only increased along the $y$ direction while the coverage along the $x$ direction remains the same. This is because NHS-OFDM with parallel pairing has the same BER performance as HS-OFDM at $y = 2.5$ m [21]. The major and minor axes of the ellipse are 2.6 and 2.2 m, respectively, and hence the area is 4.5 $m^2$, suggesting a coverage improvement of about 18.4%. Moreover, the coverage circle utilizing NHS-OFDM with cross pairing has a radius of 1.3 m and the area is 5.3 $m^2$. As a result, a further 17.8% coverage improvement is obtained using cross pairing. It can also be observed that substantial coverage improvements can be achieved when the ImR is replaced by an ImADR. For a rhombic LED placement, as can be observed from Fig. 8(b), the coverage contours employing HS-OFDM and NHS-OFDM can all be approximated as ellipses. Similarly, the smallest coverage is attained by HS-OFDM, while NHS-OFDM with cross-pairing outperforms NHS-OFDM with parallel pairing in terms of covered area. It can be seen from Figs. 8(a) and 8(b) that LED pairing and receiver type are two key factors that determine the communication coverage of MIMO-VLC systems based on NHS-OFDM in typical indoor environments. By selecting a proper LED pairing scheme and a high-performance optical receiver, the communication coverage of indoor MIMO-VLC systems based on NHS-OFDM can be maximized.

Besides LED pairing and receiver type, the output optical power of each LED is another key factor that needs to be examined. Figure 9 shows the relationship between the covered area and the LED output optical power in the indoor four-channel imaging MIMO-VLC system using HS-OFDM and cross-pairing-based NHS-OFDM at a target BER of $3.8 \times 10^{-3}$. For a square LED placement, as shown in Fig. 9(a), the covered area continuously increases with the increase of the LED output optical power. When the LED output optical power is 12 W and an ImR is used, the covered areas using HS-OFDM and cross-pairing-based NHS-OFDM are 5.7 and 8.0 $m^2$, resulting in a coverage improvement of about 40.3%. In addition, the covered areas are significantly increased when the ImR is replaced by an ImADR. For example, the covered area utilizing cross-pairing-based NHS-OFDM with an LED output optical power of 12 W is increased to 18.1 $m^2$ when an ImADR is utilized, corresponding to a 126.3% coverage area improvement in comparison to that using an ImR. When the four LEDs are placed in a rhombus, as shown in Fig. 9(b), the coverage improvements of 41.7% and 32.5% are achieved by replacing HS-OFDM with cross-pairing-based NHS-OFDM using an ImR and ImADR with an LED output optical power of 12 W, respectively. Hence, the four-channel imaging MIMO-VLC system, with either a square or rhombic LED placement, achieves the largest communication coverage using cross-pairing-based NHS-OFDM with an ImADR.

## V. Conclusion

In this paper, we have presented a comprehensive analysis of the performance of an indoor imaging MIMO-VLC system from the coverage perspective. Considering that the LEDs are used for simultaneous illumination and communication, both the illumination and communication coverages are analyzed. The square and rhombic LED placements, each consisting of four LEDs, are considered in the analysis, corresponding to the widely used square and hexagonal LED layouts. It has been shown that the illumination coverage of an MIMO-VLC system is mainly affected by the LED placement and the maximum luminous intensity of the LED. Moreover, due to the pairwise transmission nature of NHS-OFDM, two LED pairing schemes, including parallel and cross pairing, are investigated. We further show that the communication coverage of an MIMO-VLC system using NHS-OFDM is mainly determined by the LED placement, LED pairing schemes, LED output optical power, and the performance of the receiver. Detailed comparisons are conducted in terms of

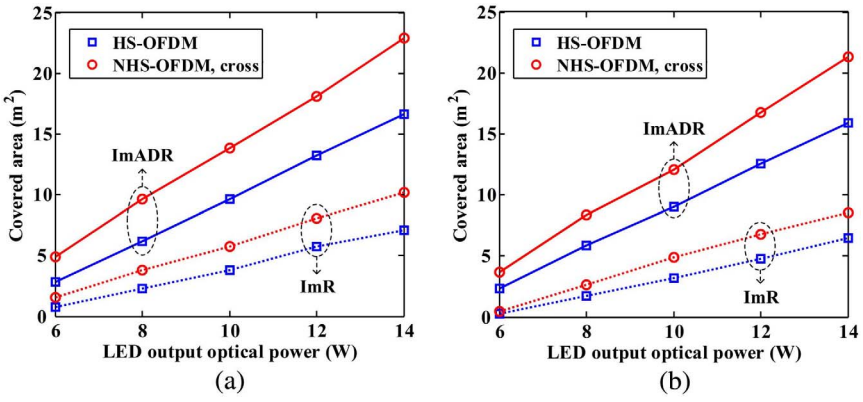


Fig. 9. Communication coverage area versus LED output optical power at a target BER of $3.8 \times 10^{-3}$ for (a) square LED placement and (b) rhombic LED placement.

two modulation techniques (HS-OFDM and NHS-OFDM), two types of optical receivers (ImR and ImADR), and two LED placements (square and rhombus) in an indoor four-channel imaging MIMO-VLC system. The obtained results demonstrate that NHS-OFDM with cross pairing using an ImADR achieves the largest communication coverage in the indoor four-channel imaging MIMO-VLC system, with either a square or rhombic LED placement.

This analysis outlines a general framework for evaluating the illumination and communication coverages of an indoor MIMO-VLC system. The obtained analytical results can be very useful for the development of practical indoor MIMO-VLC systems. In this work, the MIMO-VLC system is assumed to be ICI-free with an ideal channel matrix. In our future work, we will use ray-tracing software to simulate the overall system and get the realistic channel matrix for more practical performance analysis. Moreover, the light-reflection effects from the ceiling and the walls within the room will be investigated. The coverage of a multi-cell MIMO-VLC system will also be considered where intercell interference is a critical issue that might significantly degrade the system performance.

## Acknowledgment

This work was supported by a MOE/NTU AcRF Tier 1 Grant RG 85/13. Portions of this work were presented at the 2nd Workshop on Optical Wireless Communications (OWC), IEEE ICC 2016, titled “Communication coverage improvement of indoor SDM-VLC system using NHS-OFDM with a modified imaging receiver”.

## References

[1] R. D. Dupuis and M. R. Krames, “History, development, and applications of high-brightness visible light-emitting diodes,” *J. Lightwave Technol.*, vol. 26, no. 9, pp. 1154–1171, 2008.

[2] T. Komine and M. Nakagawa, “Fundamental analysis for visible-light communication system using LED lights,” *IEEE Trans. Consum. Electron.*, vol. 50, no. 1, pp. 100–107, 2004.

[3] S. Arnon, Ed., *Visible Light Communication*. Cambridge, UK: Cambridge University, 2015.

[4] H. Haas, L. Yin, Y. Wang, and C. Chen, “What is LiFi?” *J. Lightwave Technol.*, vol. 34, no. 6, pp. 1533–1544, 2016.

[5] H. Burchardt, N. Serafimovski, D. Tsonev, S. Videv, and H. Haas, “VLC: Beyond point-to-point communication,” *IEEE Commun. Mag.*, vol. 52, no. 7, pp. 98–105, 2014.

[6] H. Yang, J. Bergmans, T. Schenk, J. Linnartz, and R. Rietman, “Uniform illumination rendering using an array of LEDs: A signal processing perspective,” *IEEE Trans. Signal Process.*, vol. 57, no. 3, pp. 1044–1057, 2009.

[7] L. Zeng, D. O’Brien, H. Minh, G. Faulkner, K. Lee, D. Jung, Y. Oh, and E. Won, “High data rate multiple input multiple output (MIMO) optical wireless communications using white led lighting,” *IEEE J. Sel. Areas Commun.*, vol. 27, no. 9, pp. 1654–1662, 2009.

[8] A. Burton, H. Minh, Z. Ghassemlooy, E. Bentley, and C. Botella, “Experimental demonstration of 50-Mb/s visible light communications using $4 \times 4$ MIMO,” *IEEE Photon. Technol. Lett.*, vol. 26, no. 9, pp. 945–948, 2014.

[9] Y. Wang and N. Chi, “Demonstration of high-speed $2 \times 2$ non-imaging MIMO Nyquist single carrier visible light communication with frequency domain equalization,” *J. Lightwave Technol.*, vol. 32, no. 11, pp. 2087–2093, 2014.

[10] Z. Ghassemlooy, W. Popoola, and S. Rajbhandari, *Optical Wireless Communications, System and Channel Modelling With Matlab*. London, UK: CRC Press, 2012.

[11] T. Fath and H. Haas, “Performance comparison of MIMO techniques for optical wireless communication in indoor environments,” *IEEE Trans. Commun.*, vol. 61, no. 2, pp. 733–742, 2013.

[12] Y. Hong, T. Wu, and L.-K. Chen, “On the performance of adaptive MIMO-OFDM indoor visible light communications,” *IEEE Photon. Technol. Lett.*, vol. 28, no. 8, pp. 907–910, 2016.

[13] F. Jiang, H. Deng, W. Xiao, S. Tao, and K. Zhu, “An ICA based MIMO-OFDM VLC scheme,” *Opt. Commun.*, vol. 347, pp. 37–43, 2015.

[14] A. Nuwanpriya, S. Ho, and C. S. Chen, “Indoor MIMO visible light communications: Novel angle diversity receivers for mobile users,” *IEEE J. Sel. Areas Commun.*, vol. 33, no. 9, pp. 1780–1792, 2015.

[15] P. Mmbaga, J. Thompson, and H. Haas, “Performance analysis of indoor diffuse VLC MIMO channels using angular diversity detectors,” *J. Lightwave Technol.*, vol. 34, no. 4, pp. 1254–1266, 2016.

[16] A. H. Azhar, T.-A. Tran, and D. O’Brien, “A gigabit/s indoor wireless transmission using MIMO-OFDM visible-light communications,” *IEEE Photon. Technol. Lett.*, vol. 25, no. 2, pp. 171–174, 2013.

[17] P. Butala, H. Elgala, and T. Little, “Performance of optical spatial modulation and spatial multiplexing with imaging receiver,” in *Proc. IEEE Wireless Communication Networking Conf. (WCNC)*, 2014, pp. 394–399.

[18] T. Chen, L. Liu, B. Tu, Z. Zheng, and W. Hu, “High-spatial-diversity imaging receiver using fisheye lens for indoor MIMO VLCs,” *IEEE Photon. Technol. Lett.*, vol. 26, no. 22, pp. 2260–2263, 2014.

[19] A. Vavoulas, H. Sandalidis, T. Tsiftsis, and N. Vaiopoulos, “Coverage aspects of indoor VLC networks,” *J. Lightwave Technol.*, vol. 33, no. 23, pp. 4915–4921, 2015.

[20] C. Chen, W.-D. Zhong, and D. Wu, “Communication coverage improvement of indoor SDM-VLC system using NHS-OFDM with a modified imaging receiver,” in *Proc. IEEE Int. Conf. Communication (ICC) Workshops*, 2016, pp. 315–320.

[21] W.-D. Zhong, C. Chen, and D. Wu, “Non-Hermitian symmetry OFDM for indoor space division multiplexing visible light communications (invited paper),” in *Proc. Int. Conf. Transparent Optical Networking (ICTON)*, 2016, paper Mo.C2.3.

[22] C. Chen, W.-D. Zhong, and D. Wu, “Non-Hermitian symmetry orthogonal frequency division multiplexing for multiple-input multiple-output visible light communications,” *J. Opt. Commun. Netw.*, vol. 9, no. 1, pp. 36–44, 2017.

[23] E. Basar, E. Panayirci, M. Uysal, and H. Haas, “Generalized LED index modulation optical OFDM for MIMO visible light communications systems,” in *Proc. IEEE Int. Conf. Communication (ICC)*, 2016, pp. 1–5.

[24] T. Narasimhan, R. Tejaswi, and A. Chockalingam, “Quad-LED and dual-LED complex modulation for visible light communication,” arXiv:1510.08805 (2015).

[25] A. Jovicic, J. Li, and T. Richardson, “Visible light communication: Opportunities, challenges and the path to market,” *IEEE Commun. Mag.*, vol. 51, no. 12, pp. 26–32, 2013.

[26] C. Chen, W.-D. Zhong, D. Wu, and Z. Ghassemlooy, "Wide-FOV and high-gain imaging angle diversity receiver for indoor SDM-VLC systems," *IEEE Photon. Technol. Lett.*, vol. 28, no. 19, pp. 2078–2081, 2016.

[27] M. Z. Afgani, H. Haas, H. Elgala, and D. Knipp, "Visible light communication using OFDM," in *Proc. Int. Conf. Testbeds Research Infrastructures Development Networks Communities (TRIDENTCOM)*, 2006, pp. 129–134.

[28] H. Kim, D. Kwon, S. Yang, Y. Son, and S. Han, "Channel assignment technique for RF frequency reuse in CA-VLC-based accurate optical indoor localization," *J. Lightwave Technol.*, vol. 32, no. 14, pp. 2544–2555, 2014.

[29] P. Djahani and J. Kahn, "Analysis of infrared wireless links employing multibeam transmitters and imaging diversity receivers," *IEEE Trans. Commun.*, vol. 48, no. 12, pp. 2077–2088, 2000.

[30] I. Stefan and H. Haas, "Analysis of optimal placement of LED arrays for visible light communication," in *Proc. IEEE Vehicular Technology Conf. (VTC)*, 2013, pp. 1–5.

[31] "Lighting of Indoor Work Places," European Standard EN 12464-1, Jan. 2009.

[32] S. Rajbhandari, J. McKendry, J. Herrnsdorf, H. Chun, G. Faulkner, H. Haas, I. Watson, D. O'Brien, and M. Dawson, "A review of gallium nitride LEDs for multi-gigabit-per-second visible light data communications," *Semicond. Sci. Technol.*, vol. 32, no. 2, 023001, 2017.

[33] K. Cho and D. Yoon, "On the general BER expression of one- and two-dimensional amplitude modulations," *IEEE Trans. Commun.*, vol. 50, no. 7, pp. 1074–1080, 2002.

[34] H. Le-Minh, D. O'Brien, G. Faulkner, L. Zeng, K. Lee, D. Jung, and Y. Oh, "High-speed visible light communications using multiple-resonant equalization," *IEEE Photon. Technol. Lett.*, vol. 20, no. 14, pp. 1243–1245, 2008.

[35] C. Chen, W.-D. Zhong, and D. Wu, "Indoor OFDM visible light communications employing adaptive digital pre-frequency domain equalization," in *Proc. Conf. Lasers and Electro-Optics (CLEO)*, 2016, paper JTh2A.118.